A full-scale experimental study of sub-slab pressure fields induced by underground perforated pipes as a soil depressurisation technique in radon mitigation

DOI: https://doi.org/10.1016/j.jenvrad.2020.106420

Authors:

Borja Frutos [a], Isabel Sicilia [a], Oscar Campo [a], Sofía Aparicio [b], Margarita González [b], José Javier Anaya [b]; Daniel Rábago [c] and Carlos Sainz [c]

[a] Eduardo Torroja Institute for Construction Science, IETcc (National Research Council, CSIC), Madrid, Spain; borjafv@ietcc.csic.es; i.sicilia@csic.es; ocampovega@outlook.com (present Address).

[b] Leonardo Torres Quevedo Institute for Physical and Information Technologies (ITEFI, National Research Council, CSIC), Madrid, Spain; sofia.aparicio@csic.es; m.g.hernandez@csic.es; jj.anaya@csic.es

[c] Radon Group, University of Cantabria, Santander, Spain. rabagod@unican.es; carlos.sainz@unican.es

* Correspondence: borjafv@ietcc.csic.es. Eduardo Torroja Institute for Construction Science, IETcc-CSIC. C/ Serrano Galvache 4, MADRID 28033. SPAIN

Keywords: radon mitigation; soil depressurisation system; perforated pipe system; gravel bed; full-scale concrete slab; multi-sensor monitoring system.

ABSTRACT

Sub-slab depressurisation systems have proven to effectively mitigate radon entry. A poor understanding of the fluid physics underlying the technique has been shown to lower the success rate substantially. This article describes a study of pressure fields in a sub-slab gravel bed induced by a soil depressurisation system consisting of perforated pipes run under the slab at a depth of 75 cm. The advantage of the approach is that pipes can be laid from outside the building to be protected. The study was conducted on a large-scale experimental facility where the variations in morphology and scope of pressure fields with different pipe combinations could be monitored and characterised. The findings showed that pressure was uniform across the entire area in the gravel bed, whereas the sensors buried in natural soil showed pressure to depend on distance from the source. Pressure transfer to the sub-slab plane was also observed to vary depending on the active pipe. Air-flow resistance studies in the layers of soil lying between the pipes and the gravel delivered different results for each pipe. That finding would appear to be related to the presence of preferential pathways in some parts of the soil. Total pressure when several pipes were activated was observed to be practically the same as the sum of the pressures transferred by each when working separately. The correlation between extraction fan power and pressure generated was also analysed. These and other factors are discussed and analysed from a perspective of the understanding of such highly effective techniques.

1. INTRODUCTION

The identification of radon gas (Rn-222) as the second most frequent cause of lung cancer after smoking (IARC, 1998; WHO, 2009) has inspired many studies on its occurrence in residential environments (Gaskin et al., 2018; Ruano-Ravina et al., 2003). Radon is the natural decay product of radium-226, an element widespread in the Earth's crust (Nazaroff et al., 1988). Exhalation from the soil is determined by substrate permeability, which governs advective gas mobility through the pores, along with its radium content and diffusivity (Friedmann et al., 2017; Neznal and Neznal, 2005). As a gas, radon is highly mobile and can penetrate buildings across fissures or cracks or permeable materials in contact with the soil. Earlier studies have explored the mechanics of gas movement from the soil to indoor areas based on convection and diffusion physics applied to materials, geometries and areas (Collignan et al., 2012; Font and Baixeras, 2003; Garbesi et al., 1999; Hintenlang, 1992; Vasilyev and Zhukovsky, 2013).

One of the most widespread and successful protection techniques (Roserens et al., 2000) used to reduce the flow of radon into buildings is soil depressurisation (SD) (Abdelouhab et al., 2010; Cosma et al., 2015; Frutos Vazquez et al., 2011; Fuente et al., 2019b; Scivyer, 2013). Effective depressurisation with the technique calls for an in-depth understanding of the parameters involved in gas mobility in soil (Jiránek et al., 2008).

SD is deployed to depressurise the soil under the entire area of a building slab (Health Canada, 2010), thereby inverting the pressure gradient between soil and building and consequently lowering advective radon flow. System efficacy for a given area depends on the area covered by the pressure field and its intensity. Both are clearly related to substrate air-flow resistance. Substrate permeability or the presence of sub-slab obstacles such as foundation lines are factors to be borne in mind in efficacy studies. Some of the effects of those characteristics have been studied with simulated models (Bonnefous et al., 1992; Diallo et al., 2015; Gadgil et al., 1991; Muñoz et al., 2017; Reddy et al., 1991). Entry rates across construction joints or accidental cracks in the slab have likewise been analysed (Andersen, 2001; Nazaroff, 1988).

The presence of negative pressure fields is favoured by more permeable sub-slab fill material such as gravel and hindered by compact natural soil (Diallo et al., 2018; Fuente et al., 2019a; Gadgil et al., 1991; Hung et al., 2019, 2018a). Pressure field constraint has also been observed when a slab fails to ensure impermeability between the soil and the indoor space (EPA Environmental Protection Agency., 1994; Frutos and Muñoz, 2018). Leaks through joints or cracks may connect the soil and indoor space, lowering the power of the air extraction system.

An understanding of those matters helps optimise depressurisation system design. Some have been studied experimentally by analysing the pressure fields associated with different slab/soil conditions (Collignan et al., 2004; Reddy et al., 1991; Robinson, 1996) and activating the system with sumps. In contrast, here the facility used consisted of perforated pipes (of the sort normally used for drainage). The aim was to furnish supplementary information as an aid to the design of such systems, for the experimental results differ when suction is applied through linear elements such as perforated pipes rather than discrete components such as sumps.. The advantage to the former is that the pipes can be run underneath the foundations from outside the building.

The aim here was to further the understanding of pressure field behaviour in an SD system using different pipe setups. The pressure fields were characterised and data on their behaviour gathered with variations in fan power, pressure line arrangement and spacing under the slab, the number of lines deployed and the substrate type (gravel or natural soil). The study was conducted on a large-scale experimental slab, comparable to the size of the ground floor of a single family home and pressure was monitored with a double-decker sensor array.

The study of the radius of action of linear SD techniques and the variation in their pressure maps with changes in the aforementioned variables may help understand the mechanisms involved and hence optimise system design.

2. MATERIALS AND METHODS

The aim pursued was to characterise SD-induced pressure fields in the gravel and soil substrates under different linear suction conditions in a slab resting on gravel. The slab-on-gravel arrangement was chosen because it is routinely used in construction in many countries. The design flow and pressure in the depressurisation system were the only parameters analysed (Fowler et al., 1991).

The test facility, a concrete slab resting on gravel built on property belonging to the CSIC at Arganda del Rey, a town outside Madrid, was fitted with a continuous pressure monitoring system consisting in a double-decked grid of sensors positioned at two depths underneath the slab. The sensors recorded the difference between the outdoor pressure and the monitoring site value. A system of perforated pipes run into the soil parallel to the slab transferred the negative pressures generated by a mechanical extractor fan. A program using MATLAB environment (MathWorks, Natick, Massachusetts) was developed to interpret and display the pressure signals both on timelines and spatially on the slab. Substrate permeability was likewise characterised.

2.1. Concrete slab and sub-slab description

A 64 m^2 (8x8 m^2), 15 cm thick reinforced concrete slab was laid on a 20 cm thick bed of (20 mm to 40 mm) gravel. This assembly is described in the Spanish technical building code (Ministerio de Fomento, 2006), chapter DB-HS1, for non-structural slabs. The natural soil over which the gravel was laid was neither compacted nor loosened. The gravel fill was deemed to have undergone no compaction other than as induced by the weight of the concrete slab, given the nature and grain size of the stone material. The 40 cm deep by 20 cm thick perimetric foundations impeded gravel contact with elements outside the slab. A flexible plastic membrane was placed over the gravel prior to pouring the concrete to prevent collapse. Slab construction is depicted in Figure 1.

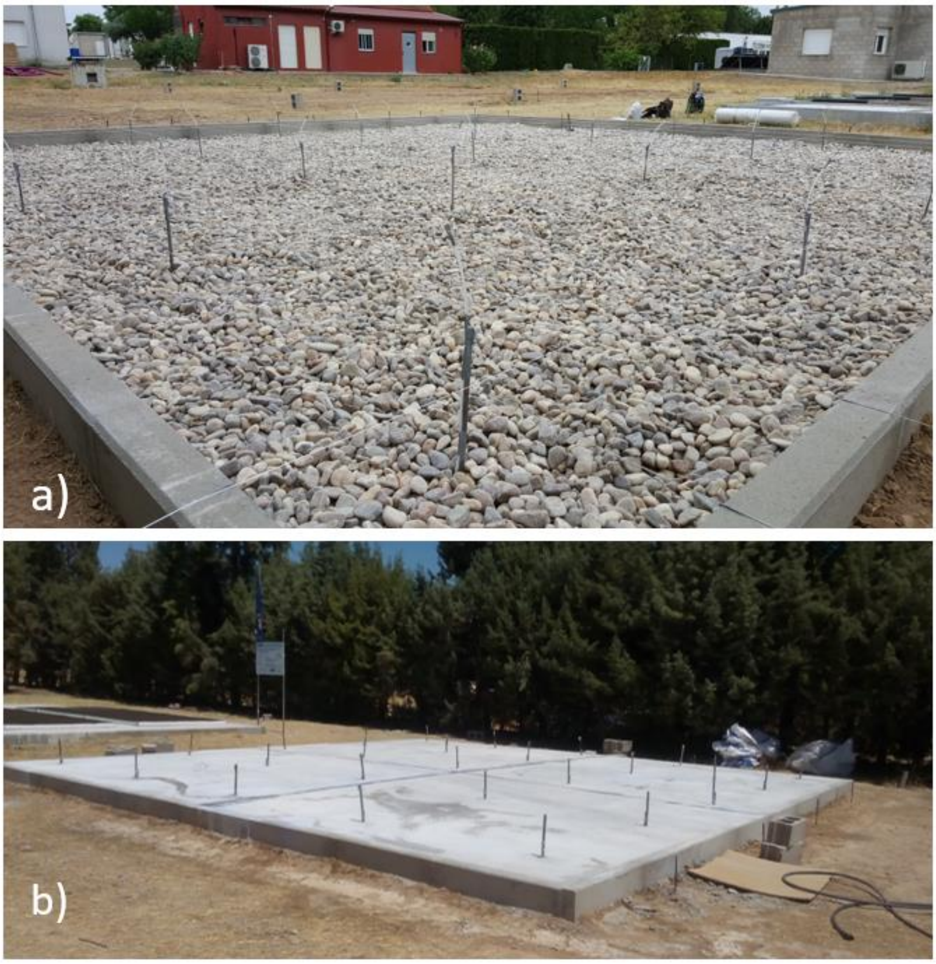

Figure 1. a) Slab construction: foundations and gravel fill; b) finished slab

Upon conclusion, the slab joints and fissures were sealed with a polyurethane sealant, fibre mesh and elastomeric paint to prevent connections between the substrate and the outdoor air. The initial post-seal tests revealed that pressures had risen on the order of two- to three-fold, confirming that such slab flaws, which are common in this type of construction, may lower depressurisation system efficacy.

The geology of the soil on which the slab was built, determined on excavated samples, was observed to consist of three layers.

Layer 1 (0-0.4 m): silty loam with some jagged edge carbonated sand, rocks and considerable peat.

Layer 2 (0.4-1.1 m): gravel and rounded rock with silty carbonated matrix.

Layer 3 (1.1-1.5 m): sandy-clayey carbonated silt with some scattered rounded gravel.

The plane 2 sensors and perforated pipes were located in layers 1 and 2; the facility did not reach into layer 3.

Soil permeability was determined in situ with the instruments developed by RADON v.o.s. (http://www.radon.eu) based on (KASˇPAR et al., 1993; Neznal and Neznal, 2005). The Radon-JOK permeameter pumps air out of the soil under constant negative pressure through a specially designed probe that interfaces with the soil across a constant and known ‘shape factor’. The probe is driven into the ground behind a sharp sacrificial tip at the forward end, generating a constant air gap. Permeability at a given depth is calculated from a formula based on Darcy's law that relates the known air flow through the probe to pumping time. With a shape factor of 0.149 m, the Radon-JOK system delivers permeability readings across a range of 10^{-11} m^2 to 10^{-14} m^2.

A total of 10 permeability measurements were carried out: 5 at a depth of about 20 cm (gravel) and 5 at a depth of 60 cm (soil), made in the center and four corners of the slab. As expected, the values were distributed more uniformly in the gravel than in the soil. As the permeability levels recorded in the gravel were higher than the upper limit of the Radon-JOK range, however, additional laboratory tests were conducted to standard ASTM D6539 (ASTM International, 2013; Fuente et al., 2019a). The mean values found were:

Gravel: K $(9.0 \pm 3.5) \times 10^{-8}$ m^2

Soil: K = (4 ± 2) x10^{-12} m^2

which lay within the range usually reported for the type of substrates at issue (Neznal et al., 2004)

2.2. Soil depressurisation system

The depressurisation system consisted of four 8 m long parallel perforated pipes spaced at 2 m on a horizontal plane 75 cm under the top of the slab. One (pipe AB), extended beyond the end of the slab, served as a control and was used to study the longitudinal pressure drop between the head and tail ends of the pipe. The findings are discussed in section 3.2.

The pipes were attached on the surface to an above-ground header pipe in turn connected to a mechanical fan that drove the system. Each perforated pipe had a cut-off valve to study the pressure fields when just one or any combination was activated.

The components of the test facility and nomenclature of the plane 1 measuring points are depicted in Figure 2. Plane 2 were labelled as in plane 1 followed by 'prime' (').

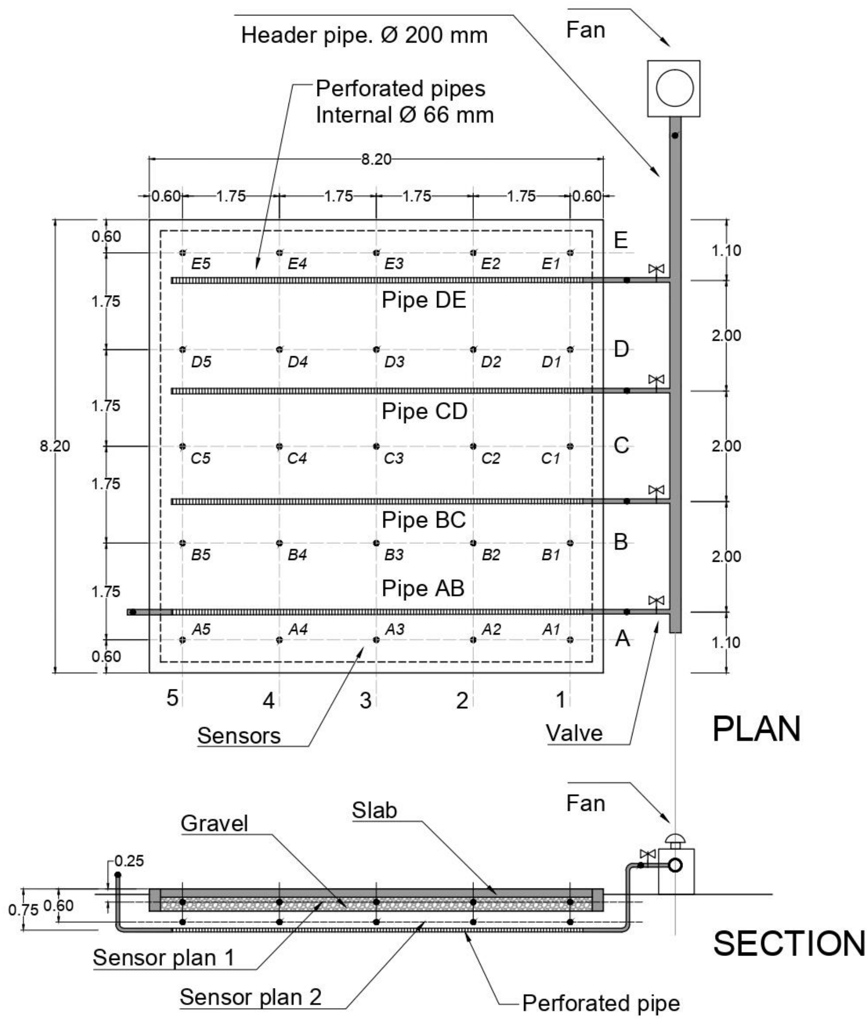

Figure 2. Plan and section views of the slab with the measuring point grid, showing depressurisation system consisting of underground perforated pipes, an above-ground collector pipe and a mechanical extractor fan. (dimension in m)

The nomenclature was defined by the intersection between lines 1 to 5 and lines A to E, whilst the perforated pipes were labelled with the letters of the two flanking longitudinal lines (AB; BC; CD; DE).

Pipe AB was not included in the experimental findings discussed in section 3 due to deviations occurring when placed in the ground.

Materials and components

- Perforated pipes: 75 mm outer and 66 mm inner diameter PVC elements, perforated with three groups of 5 cm long slots perpendicular to the length of the pipe, with the slots thus accounting for 22% of the total pipe wall area (Figure 3).

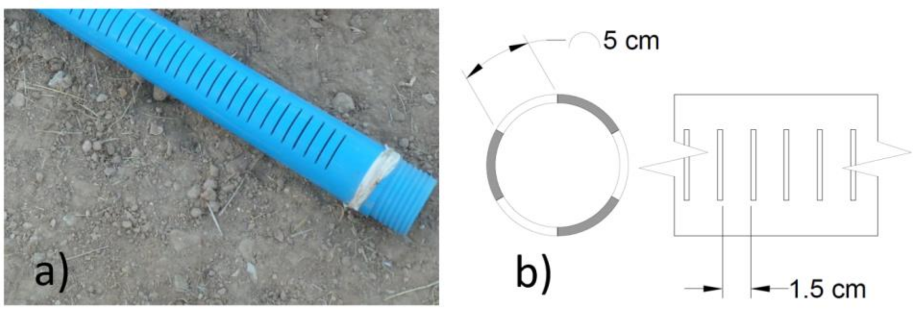

Figure 3. a) Underground perforated pipe; b) cross-section and elevation view of the pipe used

The size of the slots and their impact on pressure drop at the area adjacent to the pipe wall was studied with COMSOL Multiphysics finite element simulation software. A mean pressure dropof 27% was observed between the inside and outside of the pipe.

- 200 mm diameter PVC header pipe with blank walls (Figure 4).
- Cut-off valves on each perforated pipe for separate operation (Figure 4).
- Soler y Palau Mixvent TH-800 120 W centrifugal extractor fan; maximum air flow, 775 m^3/h; maximum pressure, 450 Pa.

A photograph of the testing facility is reproduced in Figure 4.

Figure 4. Testing facility

2.3. Multi-sensor pressure monitoring system

A number of perforated pipe setups were studied using Honeywell HSCDRRD006MDSA3 differential pressure sensors with an operating range of ±600 Pa and an accuracy of 3 Pa (Figure 2b), positioned at predetermined points on a dual-depth grid underneath the slab. Other system components included a tmux terminal multiplexer, MSP modules to connect the sensors and a LabJack U3 data acquisition unit for connection to the computer. Developed by the CSIC's Physical and Information Technologies Institute (ITEFI-CSIC), the system, along with its components and sensitivity tests, is described in Sicilia et al., 2019. A module of the pressure sensor system is shown in Figure 2b.

Readings were taken on two planes at different depths: plane 1, located at the interface between the bottom of the slab and the gravel fill, and plane 2, at 45 cm below the slab in the soil (Figure 2a). Hollow steel tubes were driven into the soil to position plane 2, and perforated plastic spheres connected to 4 mm (inner ∅) soft polyurethane tubes were used to position the plane 1 sensors.

In addition to the 25 points per plane on the 5x5 grid (Figures 5c and 2), a measuring point located outside the area covered by the slab was installed as a reference. The pressures in the fan and at the head of each pipe were also recorded.

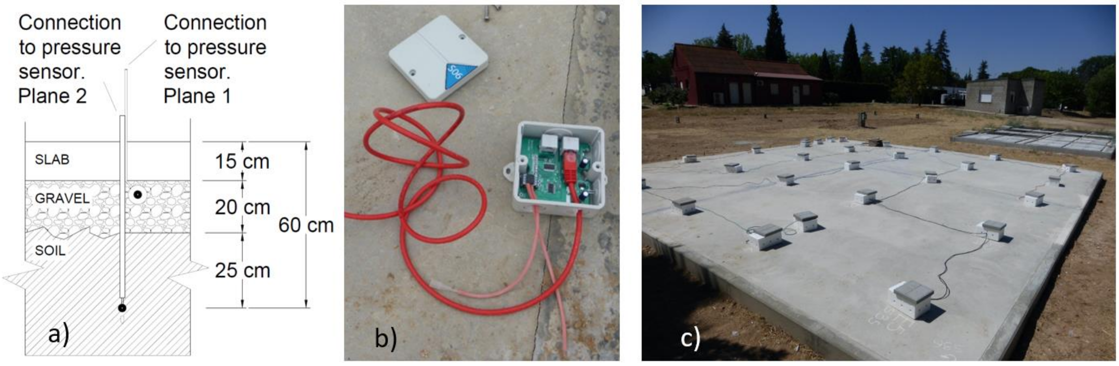

Figure 5. a) Cross-section showing pressure sensor depths; b) pressure sensor; c) finished slab with sensors in place

The differential pressure readings at each point relative to the exterior were recorded simultaneously at all points with software developed using MATLAB environment. The readings were recorded both on a timeline for each sensor and on a graphics display representing slab geometry. For further information about the visualization software see Sicilia et al., 2019.

After installing the pressure monitoring system, long-term tests were conducted to detect possible inter-sensor deviations. A sample of the findings for 5 days with the depressurisation system disconnected is reproduced in Figure 6. In this test eight sensors were positioned at different points on the slab, four in the gravel plane (A3, A5, B3, C3 in Figure 2) and four in the soil plane (B1’, B2’, C1’, C3’ in Figure 2).

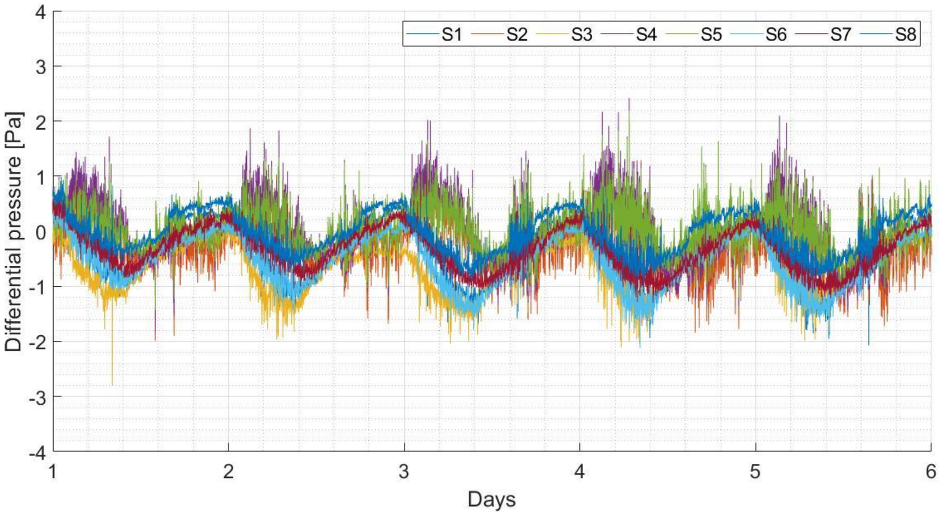

Figure 6. Pressure readings over 5 days (21 to 26 August) with depressurisation system disconnected

All the sensors were checked for performance and adjusted and calibrated where deviations were detected. Minor diurnal cycle fluctuations (±2 Pa) were observed. The difference in density between the outdoor air and the air in the soil pores due to temperature differences and the effect of thermal inertia in the soil translated into slight variations in sensor pressure readings.

The effects of atmospheric agents on the pressure between the soil and overlying space were documented in some studies (Frutos et al., 2011; Groves-Kirkby et al., 2015; Hintenlang, 1992; Yang et al., 2019; Zafrir et al., 2013). Wind action may induce momentary alterations (pressure or suction) at one end of the differential pressure device positioned on top of the slab. Here the pre-setup and system sensitivity studies revealed that rain could saturate the soil around the slab, raising the underlying pressure . In light of those considerations, all tests were conducted on similarly dry days, i.e., in the absence of rain for at least a full week. . The exposed part of the pressure device was sheltered in insulated casing to prevent superheating and direct wind action (Figures 5c and 4).

3. RESULTS AND DISCUSSION

The behaviour of the pressure field induced underneath the slab was determined under different test setups. The findings described below were applied to analyse pressure field morphology and intensity on planes 1 and 2, the pressure induced by each pipe or combination and the impact of pipe spacing and fan power. In addition, the effect of combined operation was compared to the sum of the effects of the pipes involved.

The pressure monitoring system described in section 2.3 logged the data at one reading per second, with the system programmed to record the mean of every five readings.

The procedure deployed for the experiments was as follows: no readings were taken in the first 5 min after activating the depressurisation system to ensure pressure had stabilised (which normally takes no more than 1-2 min). Data were then recorded in the following 5 min and averaged to deliver the final reading. The tests were conducted in two phases, first for plane 1 and then for plane 2. Data consistency was ensured by duplicating a four-point pressure line (B4, C4, D4, E4) and simultaneously logging the readings on both planes in every experiment.

The results of each test are discussed and analysed below.

3.1. Pipe-by-pipe pressure field distribution in planes 1 (gravel) and 2 (soil)

Seven pipe operation setups were studied. In setup 0 the fan was off; in 1 to 3 each pipe was activated separately; and in 4 through 7 different combinations of pipes were activated jointly. No results for setups involving pipe AB are reported for the reasons set out in section 2.2.

The results are summarised in Figure 7. Each matrix cell gives the findings (Pa) for the two planes: the upper value for plane 1, gravel, and the lower for plane 2, soil. The initial readings for the active pipes (BC, CD and/or DE) and for the fan are also shown. Shaded cells denote the active pipes. The pressure field morphology present in each plane and setup is readily visualised in the three-dimensional graphics on the right.

Pressure in sensors. Plane 1/Plane 2. *(Pa)*

Lines	A	B	C	D	E
5	0	0	-1	0	0
	0	x	0	0	0
4	-1	1	-1	-1	0
	0	0	0	0	0
3	0	0	-1	0	-1
	1	0	0	0	0
2	1	-1	-1	-1	0
	1	0	0	0	1
1	1	1	0	-1	0
	1	0	1	0	0

Pipes	AB	BC	CD	DE	FAN
	0	0	0	0	0

3D pressure graph *(Pa)*. P1-Gravel (orange)/P2-Soil (blue)

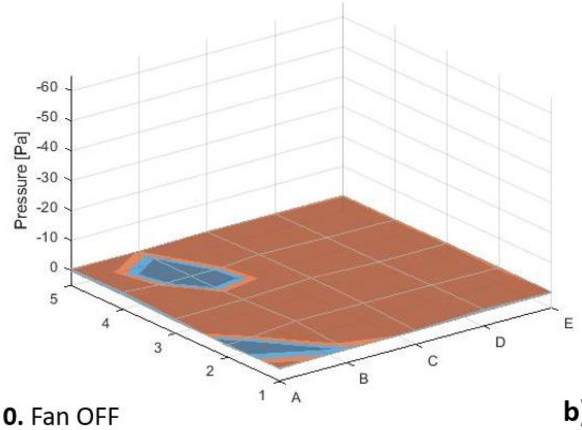

a) **Setup 0.** Fan OFF **b)**

Pressure in sensors. Plane 1/Plane 2. *(Pa)*

Lines	A	B	C	D	E
5	-11	-11	-11	-11	-11
	-5	x	-1	-8	-5
4	-11	-11	-12	-11	-11
	-5	-12	-12	-8	-7
3	-10	-11	-12	-11	-11
	-4	-20	-18	-1	-7
2	-10	-12	-12	-11	-11
	-3	-44	-7	-10	-7
1	-10	-10	-11	-11	-11
	-6	-5	-18	-10	-4

Pipes	AB	BC	CD	DE	FAN
	0	-313	0	0	-327

3D pressure graph *(Pa)*. P1-Gravel (orange)/P2-Soil (blue)

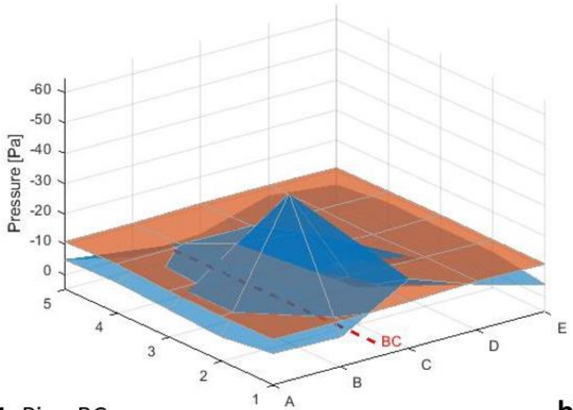

a) **Setup 1.** Pipe BC **b)**

Pressure in sensors. Plane 1/Plane 2. *(Pa)*

Lines	A	B	C	D	E
5	-6	-6	-6	-6	-6
	-2	x	-1	-8	-3
4	-6	-6	-7	-6	-6
	-2	-3	-10	-5	-4
3	-5	-6	-7	-6	-6
	-1	-4	-11	-1	-4
2	-5	-7	-6	-6	-6
	0	-7	-3	-10	-4
1	-5	-5	-5	-6	-6
	-2	0	-5	-12	-2

Pipes	AB	BC	CD	DE	FAN
	0	0	-325	0	-332

3D pressure graph *(Pa)*. P1-Gravel (orange)/P2-Soil (blue)

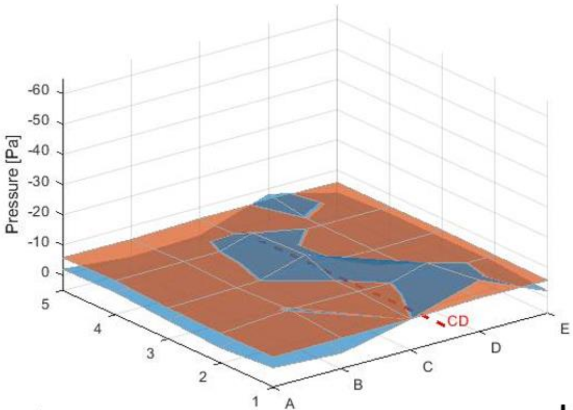

a) **Setup 2.** Pipe CD **b)**

Pressure in sensors. Plane 1/Plane 2. *(Pa)*

Lines	A	B	C	D	E
5	-34	-34	-36	-37	-39
	-17	x	-4	-25	-31
4	-35	-35	-36	-36	-37
	-17	-17	-23	-29	-52
3	-34	-35	-36	-35	-36
	-15	-21	-27	-31	-50
2	-33	-35	-35	-35	-36
	-15	-24	-26	-33	-40
1	-34	-34	-34	-35	-35
	-19	-5	-15	-33	-30

Pipes	AB	BC	CD	DE	FAN
	0	0	0	-293	-320

3D pressure graph *(Pa)*. P1-Gravel (orange)/P2-Soil (blue)

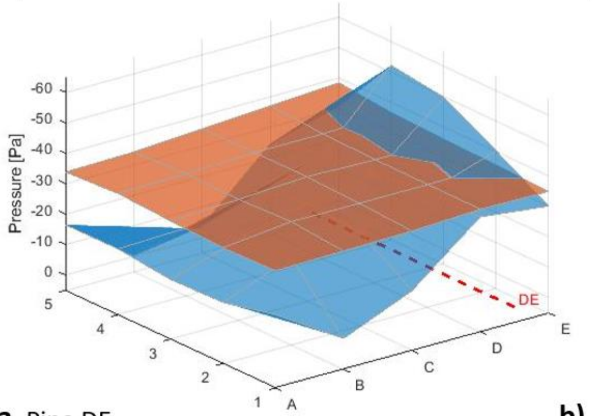

a) **Setup 3.** Pipe DE **b)**

Pressure in sensors. Plane 1/Plane 2. *(Pa)*

Lines	A	B	C	D	E
5	-51	-51	-53	-54	-56
	-24	x	-5	-39	-40
4	-51	-52	-53	-53	-53
	-25	-32	-42	-43	-65
3	-51	-52	-53	-52	-53
	-22	-45	-52	-8	-62
2	-50	-52	-52	-52	-52
	-23	-70	-37	-52	-52
1	-51	-51	-51	-52	-52
	-29	-13	-40	-56	-38

Pipes	AB	BC	CD	DE	FAN
	0	-271	-300	-289	-307

3D pressure graph *(Pa)*. P1-Gravel (orange)/P2-Soil (blue)

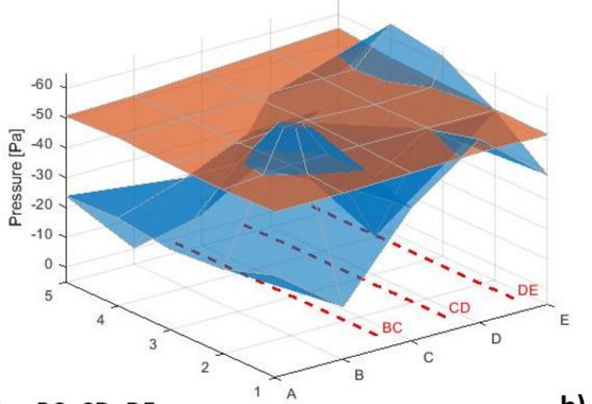

a) **Setup 4.** Pipe BC+CD+DE **b)**

Pressure in sensors. Plane 1/Plane 2. *(Pa)*

Lines	A	B	C	D	E
5	-18	-18	-19	-19	-19
	-7	x	-2	-16	-8
4	-18	-19	-19	-18	-18
	-8	-15	-21	-13	-11
3	-17	-18	-19	-18	-18
	-6	-24	-27	-2	-11
2	-17	-19	-19	-19	-18
	-6	-49	-11	-20	-10
1	-17	-17	-18	-18	-18
	-8	-6	-24	-23	-7

Pipes	AB	BC	CD	DE	FAN
	0	-304	-317	0	-321

3D pressure graph *(Pa)*. P1-Gravel (orange)/P2-Soil (blue)

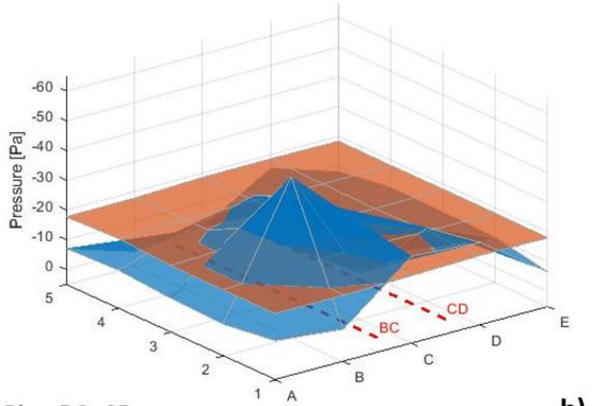

a) **Setup 5.** Pipe BC+CD **b)**

Pressure in sensors. Plane 1/Plane 2. *(Pa)*

Lines	A	B	C	D	E
5	-39	-39	-41	-42	-44
	-18	x	-4	-31	-33
4	-40	-40	-41	-41	-42
	-18	-20	-30	-34	-56
3	-39	-40	-41	-40	-41
	-16	-25	-35	-6	-54
2	-38	-41	-41	-41	-41
	-17	-29	-29	-40	-44
1	-39	-39	-39	-41	-40
	-21	-6	-20	-44	-33

Pipes	AB	BC	CD	DE	FAN
	0	0	-311	-290	-316

3D pressure graph *(Pa)*. P1-Gravel (orange)/P2-Soil (blue)

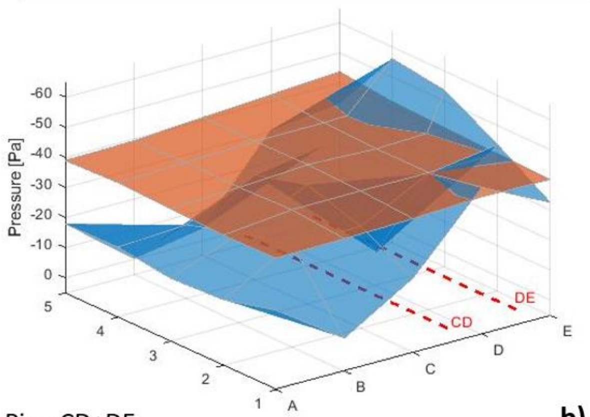

a) **Setup 6.** Pipe CD+DE **b)**

Pressure in sensors. Plane 1/Plane 2. *(Pa)*

Lines	A	B	C	D	E
5	-46	-47	-48	-49	-51
	-20	x	-4	-31	-36
4	-47	-47	-48	-48	-49
	-21	-28	-34	-36	-60
3	-46	-47	-48	-47	-48
	-18	-39	-44	-6	-57
2	-38	-41	-41	-41	-41
	-18	-64	-31	-43	-47
1	-46	-46	-46	-47	-47
	-24	-10	-33	-45	-34

Pipes	AB	BC	CD	DE	FAN
	0	-302	0	-289	-311

3D pressure graph *(Pa)*. P1-Gravel (orange)/P2-Soil (blue)

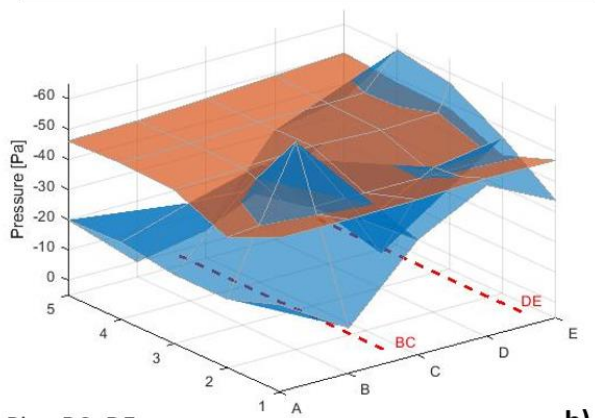

a) **Setup 7.** Pipe BC+DE **b)**

Figure 7. Pressure data in setups 0 to 7. a) pressure readings at all measuring points on both planes under different combinations of active pipes; b) 3D graphic of field morphology (orange - gravel; blue - soil)

Plane 1, gravel

One particularly prominent finding is the uniformity of pressures on the gravel plane, irrespective of the distance from the active pipe. The plane 1 values were also higher than in the soil except in sensors near the active pipe, as shown in the 3D graphics in Figure 7b and the pressure graphs in Figure 8.

Irrespective of the value observed for the active pipe, the variations recorded by the sensors across plane 1 had a standard deviation of 1 Pa, as shown in Table 1 for the three setups with a single activated pipe (1, 2 and 3), by way of illustration.

Table 1. Extracted air flow rate and pressure in active pipe, mean pressure in gravel and standard deviation, and pressure drop in 55 cm between active pipe and gravel plane

Test setup	Extract flow in pipe	Pressure in pipe	Mean pressure in plane 1, gravel		Pressure drop △P/△L
	(m^3/h)	*(Pa)*	*(Pa)*	*SD*	*(Pa/m)*
S1: pipe BC	33.7	-313	-11	1	-549.1
S2: pipe CD	18.9	-325	-6	1	-580.0
S3: pipe DE	53.1	-293	-35	1	-469.1

The pressure uniformity observed in gravel beds, a finding consistent with prior experimental research (Hung et al., 2018b), appears to be a common characteristic of such substrates, which establish a broad and uniform pressure field in depressurisation systems.

An abrupt pressure drop was observed in the 55 cm between the active pipe and the gravel plane, with a pressure drop of -468.2 (Pa/m) in the best case scenario (S3: pipe DE). Such pressure drops are routinely found in the first section of soil in depressurisation systems and are steeper in the presence of low permeability. Their intensity declines logarithmically in sections of soil at a farther distance (Gadgil et al., 1991; Health Canada, 2010). In the initial lengths the effect is reinforced by the greater pressure drop associated with the turbulence induced by greater air speed. That development was studied by factoring the Forchheimer equation into Darcy's law (Fuente et al., 2019a):

$$\frac{\Delta P}{\Delta l} = -\frac{\mu}{K_{DF}}\upsilon - c\frac{\mu}{K_{DF}}\upsilon^2$$

[1]

where K_{DF} (m^2) is Darcy-Forchheimer specific permeability and c (s/m) a constant known as the Forchheimer factor.

Significant differences in the pressure transferred to the gravel by each pipe were also observed: BC (-11 Pa); CD (-6 Pa); DE (-35 Pa). Studying variations in the behaviour of depressurisation systems with the position of the suction point, earlier authors (Frutos and Muñoz, 2018) observed a broader area to be more intensely impacted when that point was located on the perimeter, at a corner or one side, providing it was inside the slab and outward propagation was blocked by the foundation walls. In this study, pipe DE was closest to the perimeter and pipes BC and CD in inner-more positions which might partially explain the higher transfer from the former. Given the scale of the differences, however, the non-uniformity of the soil is believed to have possibly contributed to such a wide variability. As noted in section 3.1, the soil profiles revealed large gravel clusters that might well generate preferential air flow pathways between some pipes and the gravel layer. The data in Table 1 attest to an obvious relationship between extraction flows and pressure transferred to the gravel plane. Lowest resistance was found for the pipe DE setup, where transfer was highest (-35 Pa), whereas highest resistance was observed for the lowest transfer value (-6 Pa).

Plane 2, soil

Whilst the pressure distribution in gravel was very uniform at all points irrespective of the distance from the active pipe, the findings for the soil differed in that respect, with pressure varying with distance. The graphs in the figure 8 plot the pressure on both planes at a cross-section through sensor line 3 (centre of the slab) for the seven test setups. Pipe pressure is also shown.

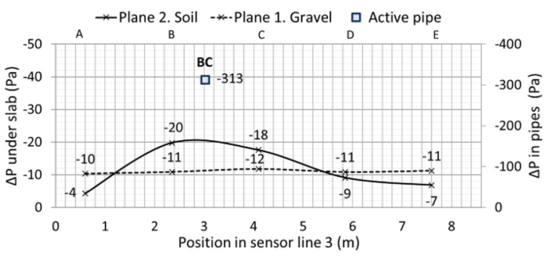

a) *Setup 1. Pipe BC*

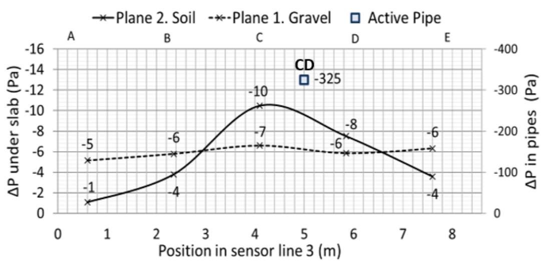

b) *Setup 2. Pipe CD*

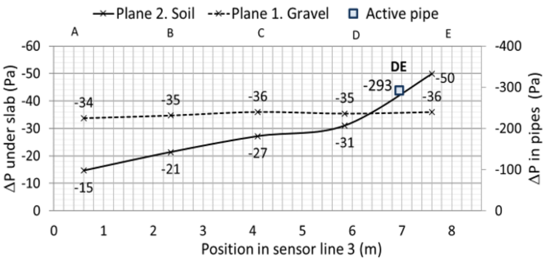

c) *Setup 3. Pipe DE*

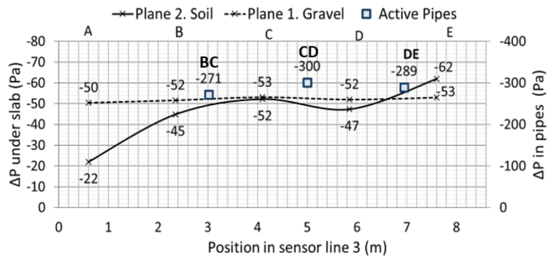

d) *Setup 4. Pipes BC+CD+DE*

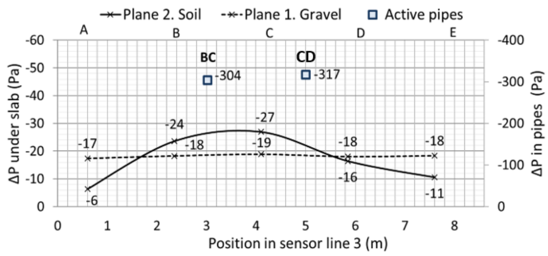

e) *Setup 5. Pipe BC+CD*

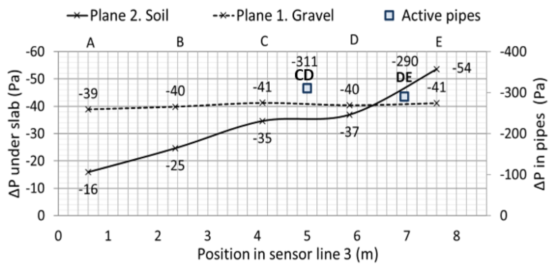

f) *Setup 6. Pipes CD+DE*

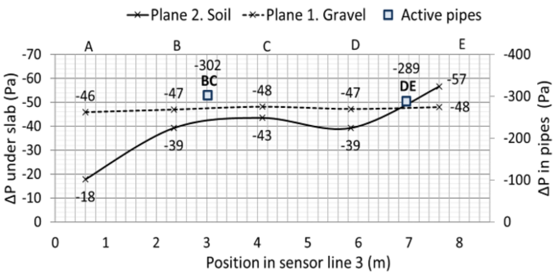

g) *Setup 7. Pipe BC+DE*

Figure 8. Differential sub-slab pressure for setups 1 through 7 at a cross-section through sensor line 3 *and pipes pressure*

The rise in pressure readings closest to the active pipe was greater in the soil than in the gravel sensors, whilst pressure drop was in keeping with the distance from the pipe/s involved in each setup (3D graphics in Figures 7b and pressure plots in Figure 8).

Although pressure varied with distance, pressure drop did not follow a uniform pattern. The data suggested that the gravel layer above may have provided an alternative pathway for pressure propagation and that the pressure detected by the soil sensors distant from the active pipe was the sum of the direct pathway and the pathway through the gravel. As noted, the latter distributed pressure evenly across the entire surface. An example of that hypothesis is shown in the diagram in Figure 9 for pipe DE, with the pathway to the farthest soil sensor, A'.

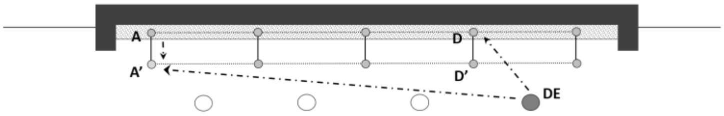

Figure 9. Possible air flow pathways from DE to A': direct, DE-A'; through gravel layer, DE-D-A-A'

An analysis of the two possible pathways provides an explanation for the pressure values observed in distant sensors, which were substantially higher than expected if only the direct pathway were followed.

3.2. Pressure distribution and pressure drop in the pipe / header pipe system

As the pressure patterns in the pipe system itself, including both above and underground components, were deemed to be of possible interest, the pressures in the aerial header (the most upstream of the components) were compared to the values in each perforated pipe in all the setups studied. As the data in Table 2 show, the pressure in the various setups, with values of 88% to 98%, were not significantly lower than in the header. All the pipes might therefore be regarded to receive around 95% of the header pressure, with no major differences observed in that regard between opening only one or any combination of pipes. That finding is promising, inasmuch as it means that a single fan would deliver sufficient pressure for a multi-pipe system with no significant pressure drop in any of the legs.

Table 2. Distribution of pressure across the pipe system for different test setups

	Pipe pressure (Pa) and % of total in header						Pipe pressure (Pa) by combination and % of total in header							
	BC		CD		DE		BC+CD+DE		BC+CD		CD+DE		BC+DE	
	(Pa)	*%*	*(Pa)*	*%*	*(Pa)*	*%*	*(Pa)*	*%*	*(Pa)*	*%*	*(Pa)*	*%*	*(Pa)*	*%*
Header	-327	100	-332	100	-320	100	-307	100	-321	100	-316	100	-311	100
BC	-313	96					-271	88	-304	95			-302	97
CD			-325	98			-300	98	-317	99	-311	98		
DE					-293	92	-289	94			-290	91	-289	93

Pressure drop across the 8 m of perforated pipe

A comparison of the readings at the head and tail ends of pipe AB (the only one fitted with a tail sensor) yielded the following data:

Head end of AB: -289.7 Pa; tail end of AB: -154.6 Pa; 53% pressure drop.

Air flow entering the pipe along its entire length would contribute to the pressure drop in such perforated elements. That observation might be of interest for perforated system design and calculation of the possible loss of efficacy with distance.

In connection with the latter concern, Figure 10 shows the pressure readings in the soil and gravel planes in longitudinal sections parallel to the active pipes, revealing pipe behaviour across its length from the header. The figure gives the initial pressure in the pipe and the value expected in each leg assuming the 53% pressure drop to be linearly distributed. Only the readings for single pipes (setups 1, 2 and 3) delivered by the longitudinal line of sensors to the right of each, i.e., line C for S1, D for S2 and E for S3, are shown.

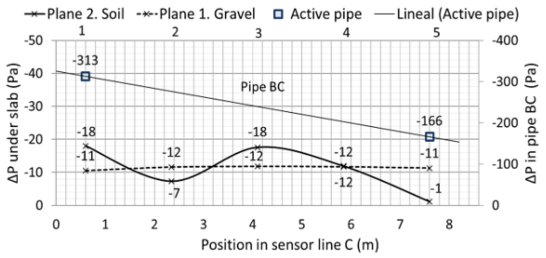

a) *Setup 1. Pipe BC*

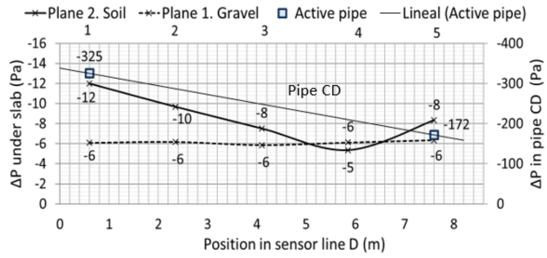

b) *Setup 2. Pipe CD*

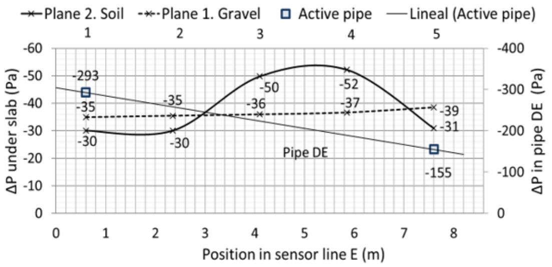

c) *Setup 3. Pipe DE*

Figure 10. Pressure graphs: a) longitudinal section along sensor line C for setup 1, b) line d for setup 2 and c) line e for setup 3

A certain decline in pressures was observed across the longitudinal section on the soil plane, although a number of points did not fit that pattern. As discussed earlier, soil non-uniformity may have induced preferential pathways between sensors in soil and the pipes.

Pressure was observed to be uniform in the gravel plane, as recorded for the overall distribution (section 3.1), with no distance-related variation in pressure.

3.3. Pressures reached by combining active pipes

The pressures reached in the gravel and soil planes when two or more perforated pipes were activated simultaneously were compared to the sum of the pressures delivered by each separately, based on the information drawn from the central line of sensors (3).

Table 3. Pressure along sensor line 3 in gravel (plane 1) and soil (plane 2), by test setup

Sensor Line 3		Individual pipes			Combinations											
		BC	CD	DE	BC+CD+DE			BC+CD			CD+DE			BC+DE		
					Sum	Real	R/S	Sum	Real	R/S	Sum	Real	R/S	Sum	Real	R/S
		(Pa)	*(Pa)*	*(Pa)*	*(Pa)*	*(Pa)*	*%*	*(Pa)*	*(Pa)*	*%*	*(Pa)*	*(Pa)*	*%*	*(Pa)*	*(Pa)*	*%*
Plane 1. Gravel	A	-10	-5	-34	-49	-50	102	-15	-17	113	-39	-39	100	-44	-46	105
	B	-11	-6	-35	-52	-52	100	-17	-18	106	-41	-40	98	-46	-47	102
	C	-12	-7	-36	-55	-53	96	-19	-19	100	-43	-41	95	-48	-48	100
	D	-11	-6	-35	-52	-52	100	-17	-18	106	-41	-40	98	-46	-47	102
	E	-11	-6	-36	-53	-53	100	-17	-18	106	-42	-41	98	-47	-48	102
Plane 2. Soil	A	-4	-1	-15	-20	-22	110	-5	-6	120	-16	-16	100	-19	-18	95
	B	-20	-4	-21	-45	-45	100	-24	-24	100	-25	-25	100	-41	-39	95
	C	-18	-10	-27	-55	-52	95	-28	-27	96	-37	-35	95	-45	-43	96
	D	-9	-8	-31	-48	-47	98	-17	-16	94	-39	-37	95	-40	-39	98
	E	-7	-4	-50	-61	-62	102	-11	-11	100	-54	-54	100	-57	-57	100

As Table 3 shows, the empirical pressure readings were practically the same as the sum of the pressures in each pipe, with a margin of error of ±5% in most cases.

In this size slab and type of gravel layer, moreover, spacing between active pipes was not a significant parameter. The pressure transferred to the gravel plane when two pipes were activated depended not on the spacing (2 m, 4 m or 6 m), but on the pressure contributed by each separately which, as discussed earlier, differed due to the non-uniformity of the substrates between pipe and slab.

The conclusion that might be drawn is that the pressures observed constitute a very close match to those found by summing the effect of each the pipes at issue, irrespective of the distance between them.

The observation to the effect that activation of a larger number of pipes entailed higher overall transfer to the gravel plane with no need to raise fan pressure also merits mention in this regard.

3.4. Relationship between fan power and pressure induced in plane 1, gravel

A potentiometer was fitted to the fan to study the pressure distribution at the lower power values normally used in depressurisation mitigation solutions.

The variation in the pressure fields beneath the slab (plane 1, gravel) was then measured under three combinations of active pipes at three potentiometer settings: 10 (the maximum), 7 and 5. The correlation between readings in the fan and in gravel is plotted in Figure 11.

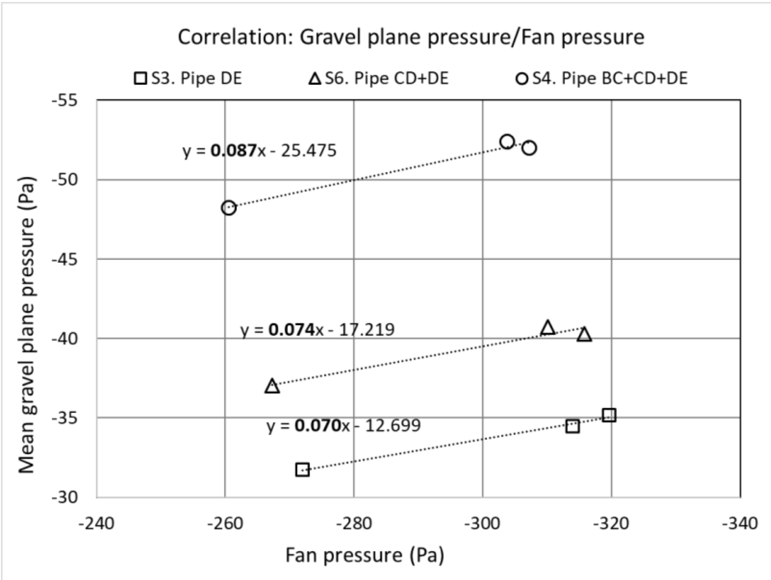

Figure 11. Gravel plane vs fan pressure in setups 3, 6 and 4

At a given fan setting, higher pressures were recorded in the soil as the number of pipes activated rose, corroborating the earlier observation to that effect (S4>S6>S3).

The data were used to study the relationship between the reduction in fan pressure and its impact on gravel plane pressure. The slope on the ($\Delta P_{GRAVEL}/\Delta P_{FAN}$) curve was observed to rise when more pipes were active, from 7.0% for pipe DE alone to 8.7% for pipe combination BC+CD+DE. That finding would appear to mean that pressure transfer to the gravel at lower fan power declined more steeply when more pipes were active.

Nonetheless, due to the narrow difference between the settings analysis was not wholly satisfactory. In future studies this effect will be verified with a more sensitive potentiometer.

4. CONCLUSIONS

Although depressurisation techniques are deemed to be highly effective, their efficacy depends on a thorough understanding of the fluid physics governing sub-slab pressure fields. Those fields were measured and characterised in this study of the depressurisation generated by a series of parallel perforated pipes underneath a large-scale slab resting on a layer of gravel. Pressure was assessed when each pipe was depressurised separately or in combination with others and at different initial pressures, controlled by a potentiometer. The conclusions drawn from the findings are set out below.

The presence of sub-slab gravel with a permeability of 10^{-8} m^2 generated a uniform pressure field across the entire 64 m^2 slab studied. That behaviour was not observed in the natural soil on plane 2, where permeability was 10^{-12} m^2 and where pressure declined with the distance from the active pipe.

This study therefore reconfirmed the benefits of gravel beds, which extend and raise the despresurisation in SD systems.

Another finding of interest was that the pressure transferred to the gravel plane varied from pipe to pipe. An analysis of the resistance in the soil between each pipe and the gravel plane revealed substantial differences that might be associated with soil non-uniformity, although pipe position relative to slab geometry might also have contributed to that result. The higher values in the outer pipes, also reported in other studies, would be due to their proximity to the foundations, which obstructed pressure field expansion on one side.

The pressure inside any given pipe did not vary when activated separately or in combination with others. At the same time, activating more pipes was found to raise sub-slab depressurisation with no need to raise the fan power. More specifically, the resulting pressure was observed to be nearly identical to the sum of the pressures of each pipe operating separately. In the slab-gravel layer arrangement studied here, that sum of pressure values was shown to depend not on inter-pipe spacing, but rather on the pressure contributed by each pipe separately. That finding may be relevant to the design of multi-pipe systems attached to a single fan, for the inference is that increasing the number of suction points or pipes is more effective than raising extraction power.

This study affords material for characterising perforated pipe-based depressurisation systems. Nonetheless, some of the matters addressed call for further research to confirm patterns and explore new areas, such as the effects of inner foundation lines on pressure propagation or performance in the absence of a gravel bed.

ACKNOWLEDGEMENTS

This research was funded by the Spanish National Research Council (CSIC) [RTC-2015-3464-5], an entity under the aegis of the country’s Ministry of Economy and Competitiveness. The study was conducted at the Eduardo Torroja Institute for Construction Science (IETcc), Spain, in conjunction with the University of Cantabria and Geocisa, S.A.

REFERENCES

Abdelouhab, M., Collignan, B., Allard, F., 2010. Experimental study on passive Soil Depressurisation System to prevent soil gaseous pollutants into building. Build. Environ. 45, 2400–2406. https://doi.org/10.1016/j.buildenv.2010.05.001

Andersen, C.E., 2001. Numerical modelling of radon-222 entry into houses: An outline of techniques and results. Sci. Total Environ. 272, 33–42. https://doi.org/10.1016/S0048-9697(01)00662-3

ASTM International, U.S., 2013. ASTM-D6539. Standard Test Method for Measurement of the Permeability of Unsaturated Porous Materials by Flowing Air.

Bonnefous, Y.C., Gadgil, A.J., Fisk, W.J., Prill, R.J., 1992. Field Study and Numerical Simulation of Sub Slab Ventilation Systems. Environ. Sci. Technol. 26, 1752–1759.

Collignan, B., Kelly, P.O., Pilch, E., 2004. BASEMENT DEPRESSURISATION USING DWELLING MECHANICAL EXHAUST VENTILATION SYSTEM, in: 4th European Conference on Protection against Radon at Home and at Work. Praha, Czech Republic.

Collignan, B., Lorkowski, C., Améon, R., 2012. Development of a methodology to characterize radon entry in dwellings 57, 176–183. https://doi.org/10.1016/j.buildenv.2012.05.002

Cosma, C., Papp, B., Cucoş Dinu, A., Sainz, C., 2015. Testing radon mitigation techniques in a pilot house from Băiţa-Ştei radon prone area (Romania). J. Environ. Radioact. 140, 141–147. https://doi.org/10.1016/j.jenvrad.2014.11.007

Diallo, T.M.O., Collignan, B., Allard, F., 2018. Analytical quantification of the impact of sub-slab gravel layer on the airflow from soil into building substructures. Build. Simul. 11, 155–163. https://doi.org/10.1007/s12273-017-0375-y

Diallo, T.M.O., Collignan, B., Allard, F., 2015. Air flow models for sub-slab depressurization systems design. Build. Environ. 87, 327–341. https://doi.org/10.1016/j.buildenv.2015.01.017

EPA Environmental Protection Agency., 1994. Making the multilateral system more effective, A TECHNICAL GUIDANCE MANUAL.

Font, L., Baixeras, C., 2003. The RAGENA dynamic model of radon generation , entry and accumulation indoors. Sci. Total Environ. 307, 55–69.

Fowler, C., Williamson, A., Pyle, B., Belzer, F., Coker, R., 1991. HANDBOOK: SUB-SLAB

DEPRESSURIZATION FOR LOW PERMEABILITY FILL MATERIAL DESIGN AND INSTALLATION OF A HOME RADON REDUCTION SYSTEM. EPA/625/6-91/029, 1991.

Friedmann, H., Baumgartner, A., Bernreiter, M., Gräser, J., Gruber, V., Kabrt, F., Kaineder, H., Maringer, F.J., Ringer, W., Seidel, C., Wurm, G., 2017. Indoor radon, geogenic radon surrogates and geology – Investigations on their correlation. J. Environ. Radioact. 166, 382–389. https://doi.org/10.1016/j.jenvrad.2016.04.028

Frutos, B., Muñoz, E., 2018. Field pressure studies for understanding depressurization techniques, in: Radon Outcomes on Mitigati on Solutions (ROOMS). Lugano.

Frutos, B., Olaya, M., Esteban, J.L., 2011. Extraction systems as construction techniques to prevent radon entry in homes. Inf. la Constr. 63, 22–36. https://doi.org/10.3989/ic.09.056

Frutos Vazquez, B., Olaya Adan, M., Quindos Poncela, L.S., Sainz Fernandez, C., Fuente Merino, I., 2011. Experimental study of effectiveness of four radon mitigation solutions, based on underground depressurization, tested in prototype housing built in a high radon area in Spain. J. Environ. Radioact. https://doi.org/10.1016/j.jenvrad.2011.02.006

Fuente, M., Muñoz, E., Sicilia, I., Goggins, J., Hung, L.C., Frutos, B., Foley, M., 2019a. Investigation of gas flow through soils and granular fill materials for the optimisation of radon soil depressurisation systems. J. Environ. Radioact. https://doi.org/10.1016/j.jenvrad.2018.12.024

Fuente, M., Rábago, D., Goggins, J., Fuente, I., Sainz, C., Foley, M., 2019b. Radon mitigation by soil depressurisation case study: Radon concentration and pressure field extension monitoring in a pilot house in Spain. Sci. Total Environ. 695, 133746. https://doi.org/10.1016/j.scitotenv.2019.133746

Gadgil, A.J., Bonnefous, Y.C., Fisk, W.J., Prill, R.J., Nematollahi, A., 1991. Influence of Subslab Aggregate Permeability On SSV Perfomance, Environmental Science and Technology. LBL-31160, Lawrence Berkeley Laboratory.

Garbesi, K., Robinson, A.L., Sextro, R.G., Nazarof, W.W., 1999. RADON ENTRY INTO HOUSES. Health Phys. 77, 183–191. https://doi.org/10.1097/00004032-199908000-00008

Gaskin, J., Coyle, D., Whyte, J., Krewksi, D., 2018. Global Estimate of Lung Cancer Mortality Attributable to Residential Radon. Environ. Health Perspect. 126, 057009. https://doi.org/10.1289/EHP2503

Groves-Kirkby, C.J., Crockett, R.G.M., Denman, A.R., Phillips, P.S., 2015. A critical analysis of climatic influences on indoor radon concentrations: Implications for seasonal correction. J. Environ. Radioact. 148, 16–26. https://doi.org/10.1016/j.jenvrad.2015.05.027

Health Canada, 2010. Reducing Radon Levels in Existing Homes. A Canadian Guide for Professional Contractors.

Hintenlang, D.E.A.-A., 1992. Pressure Differentials for Radon Entry Coupled to Periodic Atmospheric Pressure Variations. Indoor Air 1992, 208–215.

Hung, L.C., Goggins, J., Croxford, C., Foley, M., 2019. Large−scale experimental investigations of specified granular fill materials for radon mitigation by active and passive soil depressurisations. J. Environ. Radioact. 207, 27–36. https://doi.org/10.1016/J.JENVRAD.2019.05.018

Hung, L.C., Goggins, J., Fuente, M., Foley, M., 2018a. Characterisation of specified granular fill materials for radon mitigation by soil depressurisation systems. Constr. Build. Mater. 176, 213–227. https://doi.org/10.1016/j.conbuildmat.2018.04.210

Hung, L.C., Goggins, J., Fuente, M., Foley, M., 2018b. Investigation of sub-slab pressure field extension in specified granular fill materials incorporating a sump-based soil depressurisation system for radon mitigation. Sci. Total Environ. 637–638, 1081–1097. https://doi.org/10.1016/J.SCITOTENV.2018.04.401

IARC, 1998. On the evaluation of the carcinogenic risk to humans, IARC MONOGRAPHS.

Jiránek, M., Neznal, M., Neznal, M., 2008. Mitigation of ineffective measures against radon. Radiat. Prot. Dosimetry 130, 68–71. https://doi.org/10.1093/rpd/ncn120

KASˇPAR, J., PROKOP, P., MATOLÍN, M., 1993. FH-1, equipment for in situ permeability measurements, in Radon investigation in CS. Czech Geol. Surv. Spec. Pap. 4, 4–8.

Ministerio de Fomento, 2006. REAL DECRETO 314/2006, de 17 de marzo, por el que se aprueba el Código Técnico de la Edificación., REAL DECRETO 314/2006, de 17 de marzo, por el que se aprueba el Código Técnico de la Edifi- cación. https://www.boe.es/boe/dias/2006/03/28/pdfs/A11816-11831.pdf.

Muñoz, E., Frutos, B., Olaya, M., Sánchez, J., 2017. A finite element model development for simulation of the impact of slab thickness, joints, and membranes on indoor radon concentration. J. Environ. Radioact. 177, 280–289. https://doi.org/10.1016/j.jenvrad.2017.07.006

Nazaroff, W.W., 1988. Predicting the Rate of 222Rn Entry from Soil into the Basement of a Dwelling Due to Pressure-Driven Air Flow. Radiat. Prot. Dosimetry 24, 199–202. https://doi.org/10.1093/oxfordjournals.rpd.a080269

Nazaroff, W.W., Moed, B.A., Sextro, R.G., 1988. Soil as a Source of Indoor Radon, Generation, Migration, and Entry, in: Radon and Its Decay Products in Indoor W.W. Nazaroff, A.V. Nero Jr. New York, pp. 57–112.

Neznal, Matej, Neznal, Martin, 2005. Permeability as an important parameter for radon risk classification of foundation soils. Ann. Geophys. 48, 175–180. https://doi.org/10.4401/ag-3192

Neznal, Matěj, Neznal, Martin, Matolín, M., Barnet, I., Mikšová, J., 2004. New Method fro Assessing the Radon Risk of Building Sites. Czech Geol. Surv. Spec. Pap.

Reddy, T.A., Gadsby, K.J., Black, H.E., Harrje, D.T., Sextro, R.G., 1991. Modeling air flow dynamics in radon mitigation systems: A simplified approach. J. Air Waste Manag. Assoc. 41, 1476–1482. https://doi.org/10.1080/10473289.1991.10466946

Robinson, A.L., 1996. Radon Entry into Buildings : Effects of Atmospheric Pressure Fluctuations and Building Structural Factors. Thesis.

Roserens, G.-A., Johner, H.-U., Piller, G., Imbaumgarten, P., 2000. Swiss Radon Handbook. Swiss Federal Office of Public Health, Bern.

Ruano-Ravina, A., Figueiras, A., Barros-Dios, J.M., 2003. Lung cancer and related risk factors: An update of the literature. Public Health 117, 149–156. https://doi.org/10.1016/S0033-3506(02)00023-9

Scivyer, C., 2013. RADON SOLUTIONS IN HOMES Radon sump systems, GOOD REPAIR GUIDE GRG 37 Part 3.

Sicilia, I., Aparicio, S., Frutos, B., Muñoz, E., González, M., Anaya, J.J., 2019. A Multisensor System for the Characterization of the Field Pressure in Terrain. Accuracy, Response, and Adjustments. Sensors 19, 3942. https://doi.org/10.3390/s19183942

Vasilyev, A. V, Zhukovsky, M. V, 2013. Determination of mechanisms and parameters which affect radon entry into a room. J. Environ. Radioact. 124, 185–190. https://doi.org/10.1016/j.jenvrad.2013.04.014

WHO, 2009. Who Handbook on Indoor Radon - A Public Health Perspective. World Heal.

Organ. 110 p. https://doi.org/10.1080/00207230903556771

Yang, J., Busen, H., Scherb, H., Hürkamp, K., Guo, Q., Tschiersch, J., 2019. Modeling of radon exhalation from soil influenced by environmental parameters. Sci. Total Environ. 656, 1304–1311. https://doi.org/10.1016/J.SCITOTENV.2018.11.464

Zafrir, H., Barbosa, S.M., Malik, U., 2013. Differentiation between the effect of temperature and pressure on radon within the subsurface geological media. Radiat. Meas. 49, 39–56. https://doi.org/10.1016/J.RADMEAS.2012.11.019